

Conformationally Switchable Silylone: Electron Redistribution Accompanied by Ligand Reorientation around a Monatomic Silicon

Taichi Koike, Takumi Nukazawa, and Takeaki Iwamoto*



Cite This: <https://doi.org/10.1021/jacs.1c06654>



Read Online

ACCESS |



Metrics & More

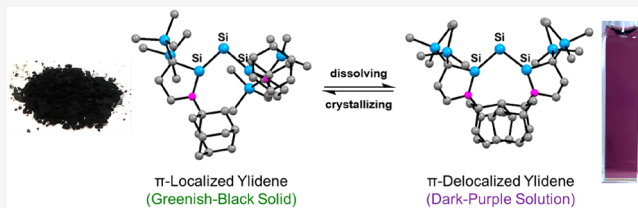


Article Recommendations



Supporting Information

ABSTRACT: Complexes that could be switched between two electronic states by external stimuli have attracted much attention for their potential application in molecular devices. However, a realization of such a phenomenon with low-valent main-group element-centered complexes remains challenging. Herein, we report the synthesis of cyclic (alkyl)(amino)silylene (CAASi)-ligated monatomic silicon(0) complexes (silylones). The bis-(CAASi)-ligated silylone adopts a π -localized ylidene structure (greenish-black color) in the solid state and a π -delocalized ylidene structure (dark-purple color) in solution that could be reversibly switched upon phase transfer (ylidene [L: \rightarrow :Si = L \leftrightarrow L = Si: \leftarrow :L]). The observed remarkable difference in the physical properties of the two isomers is attributed to the balanced steric demand and redox noninnocent character of the CAASi ligand which are altered by the orientation of the two terminal ligands with respect to the Si–Si–Si plane: twisted structure (π -localized ylidene) and planar structure (π -delocalized ylidene). Conversely, the CAASi/CDASi-ligated heteroleptic silylone (CDASi = cyclic dialkylsilylene) only exhibited the twisted π -localized ylidene structure regardless of the phase. The synthesized silylones also proved themselves as monatomic silicon surrogates. Thermolysis of the silylones in the presence of an ethane-1,2-dimine afforded the corresponding diaminosilylenes. Analyses of the products suggested a stepwise mechanism that proceeds via a disilavinylidene intermediate.

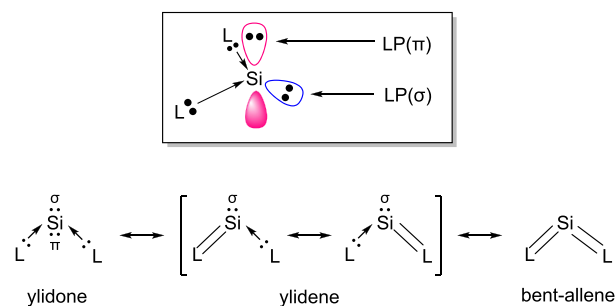


INTRODUCTION

Elemental silicon, generally known in forms such as nanostructures and bulk, has been widely applied to semiconductors and biomedicine owing to the high abundance, low toxicity, and practical electronic properties of silicon.¹ Recently, silylones, compounds with a monatomic silicon coordinated by two neutral two-electron donor ligands (general formula SiL_2 , L = two-electron donor ligand), have emerged as one of the smallest units of room-temperature-accessible elemental silicon² and as a new class of low-coordinate silicon species. They have attracted much attention due to their potential application not only as ligands complementary to carbene analogues (divalent species of group-14 elements)³ but also as surrogates of elemental silicon in a soluble form.

Since the seminal studies by Frenking and co-workers,^{4d–f} the nonclassical bonding situation of silylones has been investigated from various theoretical perspectives⁴ in analogy to their carbon analogue, carbenes which have brought to light a new field of “zerovalent group-14 element chemistry”.⁵ Considering the recent calculations independently reported by Phukan and Gadre^{4c} as well as Turek^{4a} along with the cumulative calculations, silylones have become to be understood as formal zerovalent silicon species which possess three major canonical resonance structures (Scheme 1): ylidone (L: \rightarrow :Si: \leftarrow :L), ylidene (L: \rightarrow :Si = L \leftrightarrow L = Si: \leftarrow :L), and bent allene (L = Si = L). The ylidone structure contains symmetric

Scheme 1. Symmetric Lone Pair Electrons [LP(σ)] and Antisymmetric Lone Pair Electrons [LP(π)] of a Silylone and Its Major Canonical Structures



[LP(σ)] and antisymmetric [LP(π)] lone pair (LP) electron orbitals with respect to the L–Si–L plane, and the delocalization of the LP electrons to the vacant orbital of the ligands increases the contribution of the ylidene and bent-

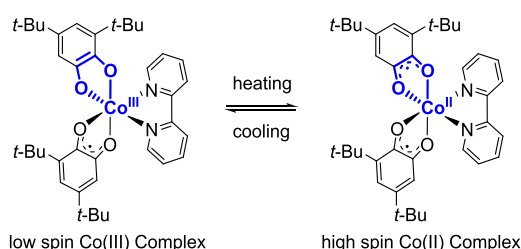
Received: June 27, 2021

allene structures. Several studies on isolable silylones⁶ along with the aforementioned theoretical studies have revealed that the major canonical structure of a silylone relies on the steric environment around the central silicon atom and the electronic effect of the ligands. However, no silylone has been reported to be switchable between two isomers with different electronic features.

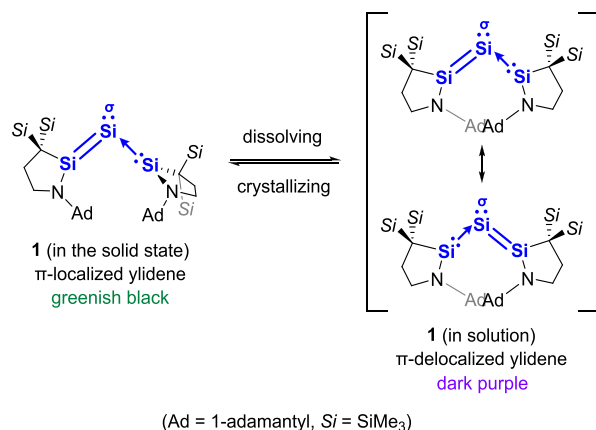
Reversible electron redistribution between a ligand and a metal center is a common strategy to switch the physical properties of transition metal complexes (Scheme 2a).⁷

Scheme 2. Examples of Switching Molecules due to Electron Redistribution of (a) Transition Metal Complexes and (b) This Work

(a) Electron Redistribution Between a Metal Center and Ligand



(b) **This Work:** Electron Redistribution Between a Silicon Center and Ligand

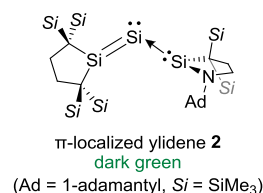


Although various switches of main-group-element species involving reactions such as intramolecular electro-/pericyclic reactions^{8a-d} and reversible dimerization^{8e-i} have been well established, realizing a molecular switch via electron redistribution between a low-valent main-group element center and a ligand remains challenging because low-valent main-group-centered complexes are typically unstable and are often irreversibly oxidized.

Herein, we report that newly synthesized silylone, that is, bis(CAASi)-ligated silylone **1** (CAASi = cyclic (alkyl)(amino)-silylene),⁹ exhibits phase-dependent isomerization via electron redistribution around the formally zerovalent silicon atom which is accompanied by a substantial change in the UV-vis absorption spectra; **1** adopts a π -localized ylidene structure in the solid state and a π -delocalized ylidene structure in solution (Scheme 2b). We envisioned that unravelling the relationship between the physical, electronic properties, and molecular structure of silylone **1** should lead to the introduction of a novel strategy to reversibly control the electronic state around main-group elements for future application to molecular devices. The details of the structure and electronic properties

of **1** will be discussed in comparison with the CAASi/CDASi-ligated (CDASi = cyclic dialkylsilylene)¹⁰ heteroleptic silylone **2** (Chart 1) and other previously reported silylones.

Chart 1. Heteroleptic Silylone 2

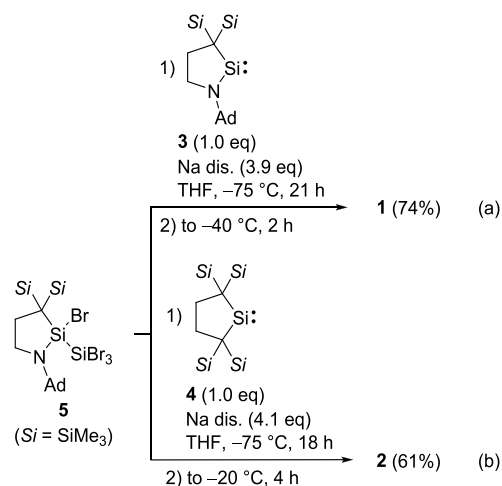


Furthermore, we discovered that **1** and **2** undergo silicon transfer reactions toward an ethane-1,2-diimine to afford the corresponding diaminosilylenes which proves the potential of **1** and **2** as a monatomic silicon surrogate.

RESULTS AND DISCUSSION

Synthesis and Single-Crystal X-ray Diffraction Analysis. Scheme 3 shows the synthesis of **1** and **2**. The treatment

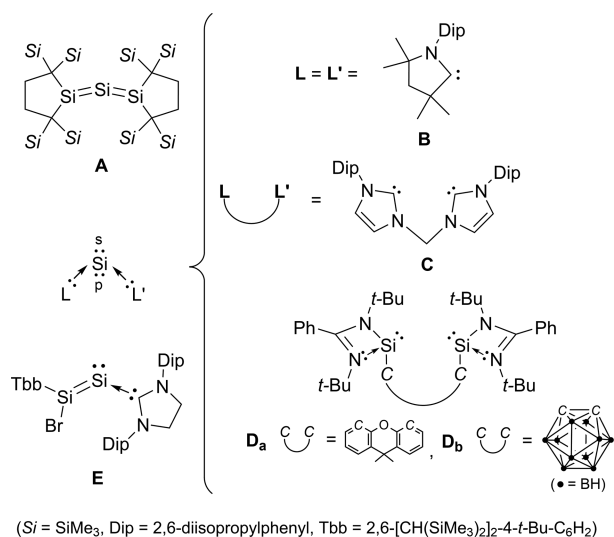
Scheme 3. Synthesis of (a) Silylones **1** and (b) **2**



of 2-bromo-2-(tribromosilyl)-1-aza-2-silacyclopentane **5** with sodium dispersion in the presence of CAASi **3** at low temperatures afforded target silylone **1** as extremely air- and moisture-sensitive greenish-black crystals in 74% yield (Scheme 3a). Similarly, **2** was synthesized as highly air- and moisture-sensitive dark-green crystals in 61% yield (Scheme 3b).¹¹ Notably, **1** exhibits greenish-black color in the solid state but dark purple in solution. Such behavior was not observed for **2** and **A** (Chart 2).^{6g}

Single crystals suitable for X-ray diffraction (XRD) analysis were obtained by recrystallization from hexamethyldisiloxane for **1** and hexane for **2** at -27 °C (Figure 1). The molecular structures show that the central silicon atom is indeed ligated by silylene **3** or **4**. Two crystallographically independent nearly identical molecules (mol. 1 and mol. 2) were observed in the asymmetric unit for **1**. The Si1-Si2-Si3 angle of **1** (mol. 1: 99.78(6)°, mol. 2: 98.29(6)°) was highly narrow and comparable to that of silylone **D_a** [103.87(3)-104.38(3)°].^{6b} Remarkably, large discrepancies in bond distances between Si1-Si2 and Si2-Si3 bonds as well as between Si1-N1 and Si3-N2 bonds were observed for **1** even though the central silicon atom was ligated by the same CAASi ligand. The Si1-

Chart 2. Examples of Structurally Related Silylones A–D and NHC-Stabilized Disilavinylidene E



Si2 bond distance of **1** [mol. 1: 2.2329(16), mol. 2: 2.2390(17) Å] fell in the longer end of typical Si=Si bonds (2.138–2.289 Å)¹² and close to those of **D** (**D_a**: 2.2451(7)–2.2586(7), **D_b**: 2.2225(6)–2.2272(6) Å).^{6a,b} The Si1–N1 bond distance [mol. 1: 1.714(4), mol. 2: 1.708(4) Å] was longer than typical Si=N bond distances [1.55–1.59 Å] but comparable to those of related compounds that possess the same CAASi moiety with a partial Si=N bond character [1.71–1.72 Å].^{9,13} Conversely, the Si2–Si3 distance [mol. 1: 2.1886(16), mol. 2: 2.1901(16) Å] was quite typical for Si=Si double bonds and close to those of **A** [2.177(1)–2.188(1) Å].^{6g} The Si3–N2 bond [mol. 1: 1.740(4), mol. 2: 1.732(4) Å] was substantially elongated compared to the Si1–N1 bond. The discrepancy in the Si–Si bond distances and the narrow Si1–Si2–Si3 angle of **1** largely differs from that of the cyclic (alkyl)(amino)carbene (CAAC)-ligated silylone **B**, exhibiting similar C–Si bond lengths [1.8411(18) Å and 1.8417(17) Å] and a wider C–Si–C bond angle [117.70(8)°].^{6c} The two five-membered rings of the terminal silylones adopted a half-chair

conformation. While the ring containing the Si3 atom was coplanar to the Si1–Si2–Si3 plane with a shorter distance to the Si2 atom, the ring containing the Si1 atom was perpendicular to the Si1–Si2–Si3 plane with a longer distance to the Si2 atom [the angle between the Si1–Si2–Si3 and C1–Si1–N1 (or C2–Si3–N2) planes, mol. 1: 81.2 (3.1)°, mol. 2: 86.3 (4.7)°]. Silylone **1** displayed a relatively planar geometry around both Si1 and Si3 atoms (Si1: 356.7° (mol. 1), 357.3° (mol. 2), Si3: 359.9° (mol. 1), 359.9° (mol. 2)).

The Si1–Si2–Si3 angle of **2** [119.62(2)°] was substantially larger than that of **1** but smaller than that of **A** [136.49(6)°].^{6b,g} As expected, a large discrepancy in bond lengths between the Si1–Si2 and Si2–Si3 bonds was observed [Si1–Si2:2.2577(5), Si2–Si3:2.1789(5) Å]. Similar to **1**, the two five-membered rings of the terminal silylones adopted a half-chair conformation. The CDASi ligand was coplanar to the Si1–Si2–Si3 plane, while the CAASi ligand was perpendicular to the Si1–Si2–Si3 plane [the angle between the Si1–Si2–Si3 and C1–Si1–N1 (or C2–Si3–C3) plane, 83.7 (11.9)°]. The Si1–N1 bond distance of **2** [1.7115(12) Å] was comparable to that of the CAASi ligand oriented perpendicular to the Si1–Si2–Si3 plane in **1**. Silylone **2** displayed a significantly pyramidalized geometry around the Si1 atom (347.1°), unlike that of the Si3 atom (359.5°).

Unlike the NHC-stabilized disilavinylidene **E** (Chart 2) reported by Filippou and co-workers¹⁴ which features a Si–C_{NHC} bond length [1.937(4) Å] typical for Si–C single bonds, the Si1–Si2 bond length in both **1** and **2** [**1** (mol. 1): 2.2329(16), **1** (mol. 2): 2.2390(16), **2**: 2.2577(5) Å] falls in the range of typical Si=Si double bonds. The aforementioned results imply that **1** and **2** both possess an electronic state different from the precedented silylones or disilavinylidene in the crystalline state and could be understood as compounds with a contribution of both ylidene and bent-allene canonical structures.

Spectroscopic Studies of Silylone 1. To gain insights into the electronic properties of **1** in the solid state, the UV–vis absorption spectrum of **1** in a KBr matrix was measured (Figure 2a).¹⁵ Silylone **1** in a KBr matrix exhibits two broad absorption bands at around 400 and 600 nm tailing up to

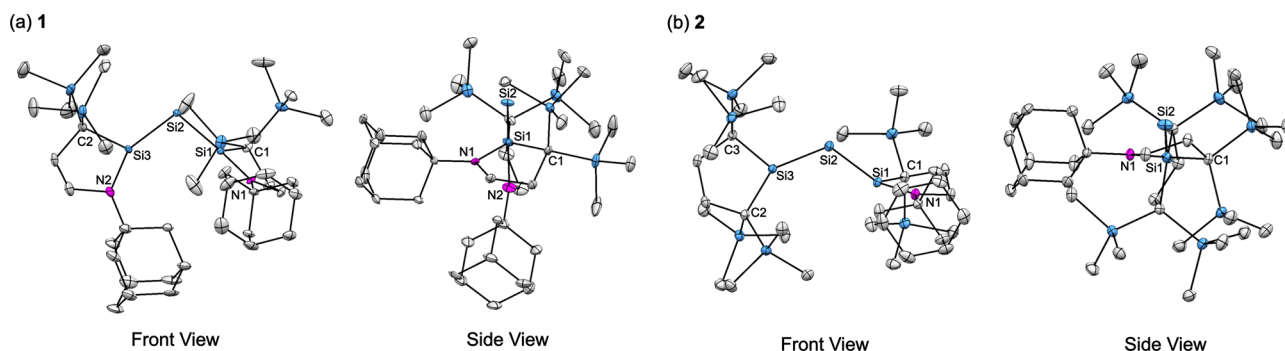


Figure 1. Molecular structures of silylones (a) **1** (mol. 1) and (b) **2** with thermal ellipsoids at 50% probability. Hydrogen atoms and **1** (mol. 2) have been omitted for clarity. Selected bond lengths [Å], bond angles [°], and dihedral angles [°]: **1** (mol. 1): Si1–Si2 2.2329(16), Si2–Si3 2.1886(16), Si1–C1 1.881(4), Si1–N1 1.714(4), Si3–C2 1.900(5), Si3–N2 1.740(4), Si1–Si2–Si3 99.78(6), C1–Si1–N1 96.24(18), C2–Si3–N2 95.76(19), N1–Si1–Si3–N2 62.4(2), N1–Si1–Si3–C2 125.3(4), C1–Si1–Si3–N2 76.7(2), C1–Si1–Si3–C2 95.6(4), **1** (mol. 2): Si1–Si2 2.2390(17), Si2–Si3 2.1901(16), Si1–C1 1.881(4), Si1–N1 1.708(4), Si3–C2 1.895(4), Si3–N2 1.732(4), Si1–Si2–Si3 98.29(6), C1–Si1–N1 95.97(18), C2–Si3–N2 95.75(19), N1–Si1–Si3–N2 62.8(2), N1–Si1–Si3–C2 128.3(4), C1–Si1–Si3–N2 71.7(2), C1–Si1–Si3–C2 97.2(4). **2**: Si1–Si2 2.2577(5), Si2–Si3 2.1789(5), Si1–C1 1.8921(14), Si1–N1 1.7115(12), Si3–C2 1.9092(14), Si3–C3 1.9072(14), Si1–Si2–Si3 119.62(2), C1–Si1–N1 95.79(6), C2–Si3–C3 99.16(6), C1–Si1–Si3–C3 83.8(1), C1–Si1–Si3–C2 95.72(8), N1–Si1–Si3–C2 84.69(8), N1–Si1–Si3–C3 95.7(1).

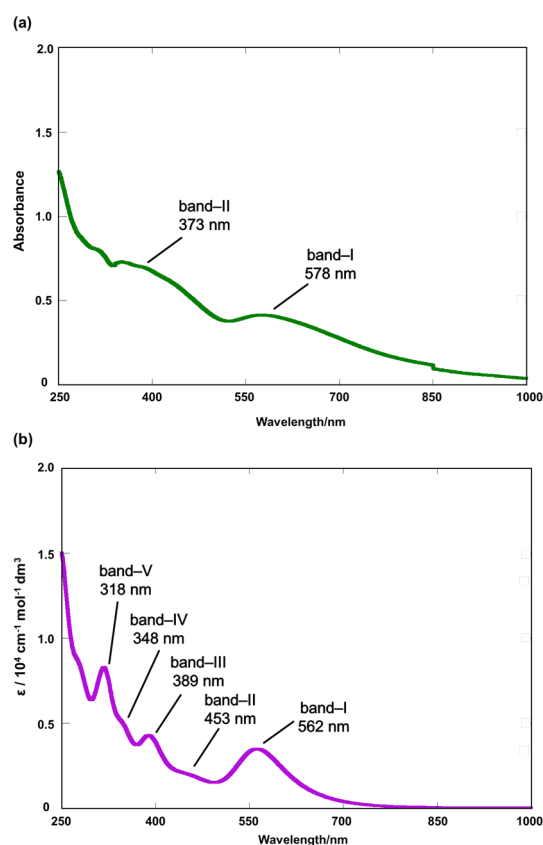


Figure 2. UV-vis spectra of silylone **1** (a) in a KBr matrix and (b) in hexane at room temperature.

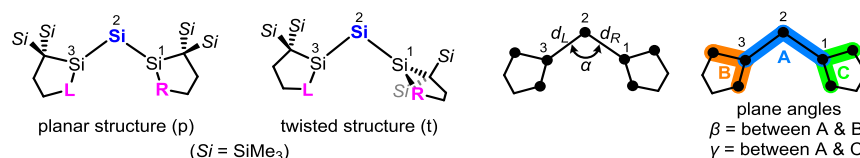
~1000 nm. The spectrum covers most of the visible region, which agrees with the intense greenish-black color in the solid state. The structural features of the optimized structure of **1** (**1_t**) calculated at the B3PW91-D3/B1 (B1 = 6-311G(d) [Si, N], and 6-31G(d) [C, H]) levels of theory were in good agreement with those of **1** obtained by XRD analysis (Table 1), and the spectral features were well reproduced by time-dependent DFT (TD-DFT) calculations of **1_t** (M06-2X/B2

(B2:6-311+G(d) [Si,N], 6-31+G(d) [C,H]) level of theory; Figure S74),¹⁶ which suggests that in the solid state **1** possesses a structure similar to that observed in the single crystal shown in Figure 1. Unfortunately, no signals could be obtained from the solid-state (CP MAS) NMR spectra measurements of **1**, prohibiting further spectroscopic studies in the solid state.

Dissolution of the greenish-black solid of **1** in hexane afforded a dark-purple solution. The UV-vis spectrum of **1** in hexane at room temperature (Figure 2b) exhibited several distinct absorptions between 300 and 600 nm [$\lambda_{\text{max}} = 562$ (band-I), 453 (band-II), 389 (band-III), 348 (band-IV), and 318 (band-V) nm] which is significantly different from that in the solid state [$\lambda_{\text{max}} = 578$ and 373 nm]. The variable-temperature (VT) UV-vis spectrum of **1** in 3-methylpentane at 93 K did not show a substantial change in spectral features compared to those at room temperature (Figure S76).

Multinuclear NMR spectra provided further insights into the structure of **1** in solution. The ²⁹Si NMR spectrum of **1** showed only two signals for the central silicon skeleton ($\delta = -95.0$ [Si-Si-Si], 164.4 ppm [terminal (alkyl)(amino)Si]), which implies that the two silicon nuclei of the terminal silylene units are equivalent on the NMR time scale. The chemical shift for the silicon nuclei of the central silicon atom was significantly upfield shifted compared to **A** ($\delta = 157$ ppm),^{6g} and the difference of the observed chemical shifts between the central and terminal silicon nuclei in **1** ($\Delta\delta = 164.4$ ppm - (-95.0 ppm) = 259.4 ppm) was substantially larger than that of **A** ($\Delta\delta = 39.9$ ppm),^{6g} which implies that **1** possesses a highly polarized bond character in solution. Notably, **1** exhibited two broad signals for the silicon nuclei of the SiMe₃ moieties ($\delta = 1.6$ and 1.7 ppm), which was also the case for the ¹H and ¹³C NMR spectra. Conversely, only one set of signals assignable to the carbon nuclei of the adamantyl or azasilacyclopentyl moieties was observed, which suggests that only the SiMe₃ moieties are unequivalent in the NMR time scale. Similar to the VT UV-vis spectroscopic studies, measurement of multinuclear VT NMR spectra at low temperatures did not show a substantial change in spectral features other than signal sharpening (Figures S16-S21).

Table 1. Selected Structural Parameters of Calculated Silylones with Planar or Twisted Structures



compound	L	R	$d_L/\text{\AA}$	$d_R/\text{\AA}$	$\alpha/^\circ$	$\beta/^\circ$	$\gamma/^\circ$	$\Delta G^{a,b}$
1_p	N-Ad	N-Ad	2.227	2.227	100.60	29.55	29.55	0.0
1_p (benzene) ^c			2.230	2.230	101.09	29.64	29.64	0.0
1_t			2.196	2.232	95.74	16.74	84.44	-0.2
1_t (benzene) ^c			2.198	2.237	96.47	17.62	83.36	4.3
6_p	N-Me	N-Me	2.221	2.221	85.90	29.06	29.07	0.0
6_t			2.201	2.221	84.19	18.70	84.34	8.3
A_t	C(SiMe) ₃	C(SiMe) ₃	2.183	2.181	133.89	48.59	43.71	-
7_p	C(SiH ₃) ₂	C(SiH ₃) ₂	2.215	2.217	107.82	29.78	34.19	0.0
7_t			2.172	2.271	95.54	15.98	78.28	10.0
8_p	CMe ₂	CMe ₂	2.217	2.217	100.01	29.85	29.84	-
2_t	C(SiMe ₃) ₂	N-Ad	2.174	2.260	117.69	1.23	89.86	-
9_t	CMe ₂	N-Me	2.190	2.243	87.07	2.87	67.16	-

^aCalculated at the B3PW91-D3/B1 level of theory. ^bAt 298.15 K, in kJ/mol. ^cSolvent = benzene.

At this point, the possibility of a fast equilibrium between the unsymmetrical twisted structures of **1** as found in the crystalline state via the rotation around the Si–Si bond could not be ruled out. However, the aforementioned spectroscopic studies as a whole brought us the idea that **1** in solution might exhibit a structure different from that in the crystalline state which was supported by DFT calculations discussed in the following section.

Structure of Silylone 1 in Solution. DFT calculation provided further insight into the structure of **1** in solution. We found another local minimum of **1** (**1_p**, Figure 3) in addition to

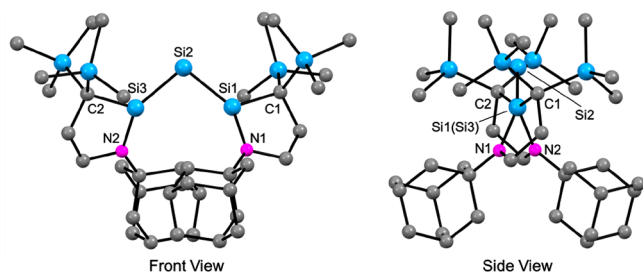


Figure 3. Calculated molecular structure of silylone **1_p**.

1_t at the B3PW91-D3/B1 (solvent = benzene) level of theory. **1_t** and **1_p** were calculated to be almost the same in relative Gibbs energies both in the gas phase and in benzene (Table 1).¹⁷ The structure of **1_p** has a local C_2 symmetry [Si1–Si2, Si2–Si3: 2.2297 Å; Si1–N1, Si3–N3: 1.7413 Å; Si1–Si2–Si3: 101.09°], which was in accordance with the spectral features observed in solution. The Si–Si distances of **1_p** were close to those of **D** (**D_a**: 2.2451(7)–2.2586(7), **D_b**: 2.2225(6)–2.2272(6) Å). Notably, the two five-membered rings of the terminal CAASi exhibited a parallel geometry [the angle between the Si1–Si2–Si3 and C1–Si1–N1 (C2–Si3–N2) planes, 29.6 (29.6)°] which largely differs from the molecular structure of **1** obtained by XRD analysis (Figure 1a). The UV–vis spectrum in solution was also well reproduced by TD-DFT calculations of **1_p** (M06-2X/B2 level of theory; Figure S74), which is completely different from the calculated band positions for **1_t**. The observed ²⁹Si signals of **1** in solution ($\delta = -95.0$ [Si–Si–Si], 164.4 ppm [(alkyl)(amino)Si]) were close to the ²⁹Si chemical shifts calculated for **1_p** [GIAO/M06-L/6-311+G(2df,p) level of theory; $\delta_{\text{calc}} = -130.6$ [Si–Si–Si], 176.3 [(alkyl)(amino)Si]¹⁸ but significantly far from those calculated for **1_t** ($\delta = -155.2$ [Si–Si–Si], 129.0 ppm [(alkyl)(amino)Si3], 187.9 ppm [(alkyl)(amino)Si1]). The two sets of signals observed for the SiMe₃ moieties should be due to the close contact of the two adamantyl moieties prohibiting the rotation of the CAASi ligands along the Si–Si bond. All of the above calculations suggest that **1_p** should most likely be the dominant structure of **1** in solution which implies that the structural change of **1** should be mainly responsible for the observed switch in optical properties.

Spectroscopic Studies of Silylone 2. As a comparison to silylone **1**, the same spectroscopic studies were conducted for silylone **2**. Figure 4 shows the UV–vis absorption spectra of **2** in a KBr matrix and in hexane at room temperature, respectively. In both cases, two distinct absorptions were observed around 400 and 600 nm [$\lambda_{\text{max}} = 605$ (band-I), 404 (band-II) nm in KBr matrix; 579 (band-I, $\epsilon = 700$), 400 (band-II, $\epsilon = 24\,000$) nm in hexane]. The band positions calculated for the optimized structure of **2** (**2_v**, M06-2X/B2//B3PW91-

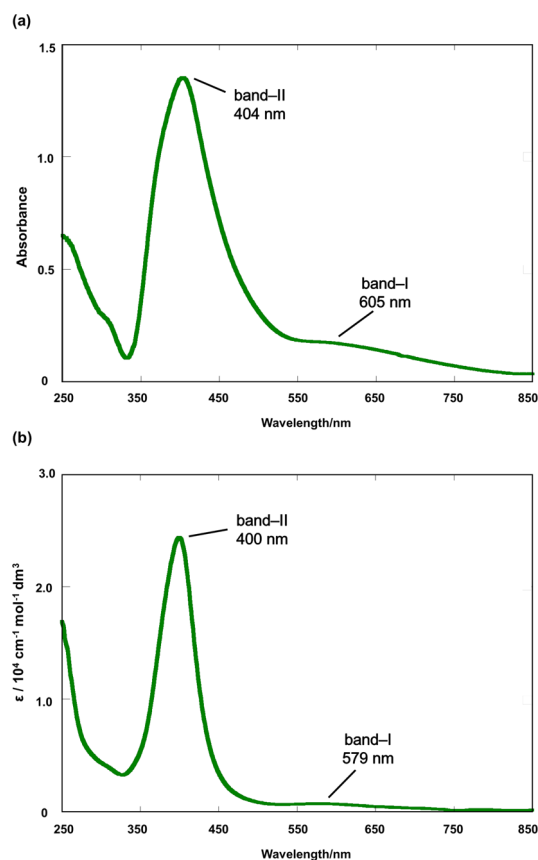


Figure 4. UV–vis spectra of silylone **2** (a) in a KBr matrix and (b) in hexane at room temperature.

D3/B1 level of theory, Figures S77–S78), which resembles the structure determined by XRD analysis, were qualitatively in good agreement with the observed spectra in the KBr matrix which suggests that in the solid state **2** possesses a structure similar to that shown in Figure 1b. Notably, the spectral features of **2** were significantly different from those of **1** but highly resemble those of **A** in hexane [$\lambda_{\text{max}}(\epsilon) = 584$ (700), 390 nm (21 300)].⁶⁸

Three signals other than those for the SiMe₃ groups were observed for **2** in the ²⁹Si NMR spectrum in benzene-*d*₆ ($\delta = 56.6$ [Si–Si–Si], 171.0 [(alkyl)(amino)Si], 191.9 ppm [(dialkyl)Si]). While the chemical shifts for the silicon nuclei of the CDASi and CAASi moieties were comparable to those for **A** ($\delta = 197$ ppm) and **1** (165 ppm),⁶⁸ that for the central silicon nuclei (56.6 ppm) was in between those of **A** ($\delta = 157$ ppm) and **1** ($\delta = -94.9$ ppm). The ²⁹Si chemical shifts calculated for **2_t** [GIAO/M06-L/6-311+G(2df,p) level of theory; $\delta_{\text{calc}} = 70.4$ [Si–Si–Si], 165.5 [(alkyl)(amino)Si], 194.9 ppm [(dialkyl)Si]] were in good agreement with the aforementioned experimental values. The above studies as a whole support the sustained structure of **2** regardless of the phase.

Investigation of the Electronic and Optical Properties by DFT Calculations. Figure 5 shows the frontier Kohn–Sham orbitals of silylones **1_p**, **1_t**, and **2_t** calculated at the M06-2X/B2//B3PW91-D3/B1 level of theory, which reflect the electron distribution of the formal LP(σ) and LP(π) electrons across the Si1–Si2–Si3 skeleton. In the case of **2_v**, the HOMO is the π (Si2 = Si3) orbital which is accompanied by the corresponding π^* orbital (LUMO+1). The HOMO–1 shows

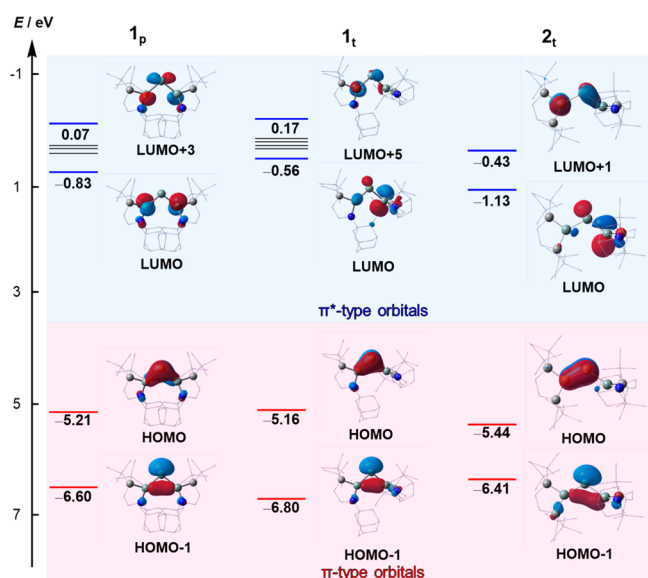


Figure 5. Selected frontier Kohn–Sham orbitals of 1_p , 1_t and 2_t calculated at the M06-2X/B2//B3PW91-D3/B1 level of theory (isosurface value = $0.05 e^-/\text{au}^3$).

the lone pair orbital of the Si2 atom substantially delocalized to the Si1 atom, while the LUMO displays the corresponding π^* -type orbital. The feature of HOMO–1 and LUMO resembles that of *trans*-bent double (slipped π) bonds. The Wiberg bond index (WBI) calculated for the Si1–Si2 bond (1.41) of 2_t is smaller than that for Si2–Si3 (1.82) but indicates a partial double bond character, which agrees with the substantial delocalization of the Si2 lone pair electrons LP(σ) to the 3p orbital on the Si1 atom found in the HOMO–1.

In contrast to 2_t , the HOMO of 1_t is the π (Si2 = Si3) orbital with a larger contribution of the Si2 atom which is accompanied by the corresponding π^* -type orbital (LUMO +5). The HOMO–1 of 1_t shows that the LP(σ) electrons of the Si2 atom only slightly delocalized to the Si1 atom, while the LUMO displays the corresponding π^* -type orbital. Although the WBI calculated for the Si1–Si2 bond (1.39) of 1_t was significantly smaller than that for Si2–Si3 (1.68), it still indicated a partial double bond character which agrees with the weak delocalization of the LP(σ) electrons to the 3p orbital of the Si1 atom found in the HOMO–1. Notably, the WBI of the Si2–Si3 bond (1.68) is smaller than that of 2_t (1.82), which is consistent with the existence of a π -donating nitrogen atom adjacent to the Si3 atom of 1_t . The weak delocalization of the LP(σ) electrons should be attributed to the narrow Si1–Si2–Si3 bond angle (95.74°) of 1_t compared to 2_t (117.69°), which could lower the energy level of the LP(σ) and weaken the effective interaction between the LP(σ) orbital and the Si1 3p orbital.

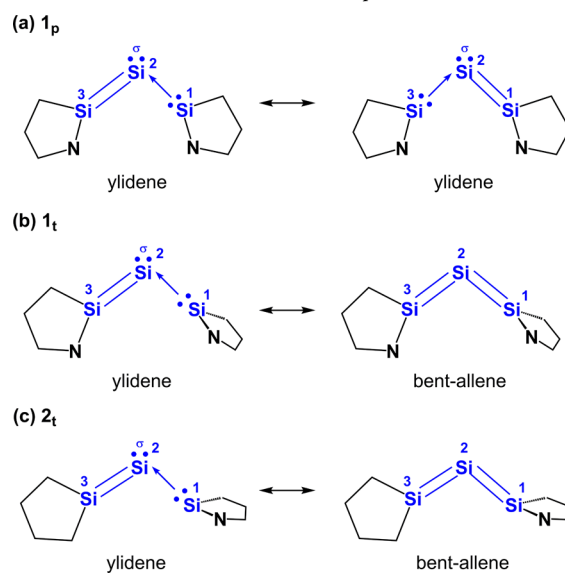
Silylone 1_p also exhibits an LP(σ) orbital for HOMO–1, while the HOMO was the LP(π) orbital substantially delocalized to both Si1 and Si3 atoms. The LUMO was an out-of-phase combination of the 3p orbitals of the two terminal CAASI moieties. The WBI of 1_p was 1.53 for both Si1–Si2 and Si2–Si3 bonds, which is in accord with the substantial delocalization of the LP(π) electrons to the vacant 3p orbitals of the Si1 and Si3 atoms seen in the HOMO.

Natural localized molecular orbital (NLMO) analysis provided further information on the electron distribution of the LP(σ) and LP(π) electrons across the Si1–Si2–Si3

skeletons. The LP(σ) electrons are mainly localized on the central silicon atom for silylones 1_p , 1_t and 2_t but delocalized more to the Si1 atoms than the Si3 atoms for 1_t and 2_t (1_p : Si3 11%, Si2 76%, Si1 11%, 1_t : Si3 5%, Si2 83%, Si1 9%, 2_t : Si3 4%, Si2 79%, Si1 14%), which agrees with the weak but significant double bond character of the Si1–Si2 bonds. The relative contribution of the Si1 atom of 2_t to LP(σ) was greater than that of 1_t , which is consistent with the stronger interaction between the LP(σ) orbital and 3p orbital of the Si1 atom for 2_t compared to that for 1_t . Perpendicular to the LP(σ) orbitals lie the LP(π) electrons. For 1_p , the two LP(π) electrons are delocalized across the Si1–Si2–Si3 skeleton where 56% of the electron density is located on the Si2 atom and 19% for both Si1 and Si3 atoms. Conversely, the two electrons of 1_t and 2_t are mainly delocalized over the Si2 and Si3 atoms (1_t : Si3 33%, Si2 56%, Si1 7%, 2_t : Si3 39%, Si2 54%, Si1 4%).

Based on the aforementioned theoretical calculations, both 1_p and 1_t possess an LP(σ) orbital, and the major electronic differences between the two silylones should be the electron distribution of the LP(π) electrons across the Si1–Si2–Si3 skeleton controlled by the orientation of the ligands (Scheme 4a and 4b). These results were also supported by NBO-based

Scheme 4. Schematic Representation of the Major Canonical Structures for Silylones 1_p , 1_t and 2_t



Natural Resonance Theory (NRT) analysis: the resonance weightings of the corresponding contributing resonance structures obtained from NRT analysis are ylidene ($2 \times 22.3\%$) for 1_p , ylidene (24.8%) + bent-allene (21.7%) for 1_t ,¹⁹ and ylidene (46.6%) + bent-allene (34.6%) for 2_t (for details, see Figures S82–S84 (NBO analysis) and S100 (NRT analysis)).²⁰ Thus, 1_p and 1_t should both be interpreted as a ylidene-type silylone but with the LP(π) electrons delocalized across the Si1–Si2–Si3 skeleton for 1_p (π -delocalized ylidene) and localized on the Si2 and Si3 atoms (π -localized ylidene) for 1_t . Although 2_t could also be interpreted as a π -localized ylidene, its electronic properties differ from that of 1_t in the amount of delocalization of the LP(σ) electrons to the 3p orbital of the Si1 atom. The larger Si1–Si2–Si3 angle of 2_t enables stronger interaction of the LP(σ) electrons with the 3p orbital of the Si1 atom, which enhances the contribution of the bent-allene character compared to 1_t (Scheme 4c). The above

results are in accord with the recent calculations reported by Turek and co-workers that the ylidene resonance structure is dominant for most heavier group-14-element zerovalent complexes, and the contribution of the ylidene or bent-allene increases depending on the ligands.^{4a}

With the above results, the UV-vis absorption spectra were revisited. The TD-DFT calculations of silylones **1_p**, **1_t**, and **2_t** imply that the absorptions in the visible region are mainly attributed to the $\pi \rightarrow \pi^*$ -type transitions between the frontier orbitals shown in Figure 5 (Tables S4–S6). Notably, a significant difference in the intensities of the longest-wavelength absorption bands was observed between the π -localized ylidene **1_t** and **2_t** and π -delocalized ylidene **1_p**. The π -localized ylidene **1_t** and **2_t** exhibit weak longest-wavelength absorption intensities due to a symmetry-forbidden transition [**2_t**, $\lambda_{\text{max,calcd}} = 720$ nm, oscillator strength (f) = 0.0005, HOMO \rightarrow LUMO];²¹ **1_t**, $\lambda_{\text{max,calcd}} = 644$ nm, $f = 0.0033$, HOMO \rightarrow LUMO], while the π -delocalized ylidene **1_p** exhibits a band with a significantly strong intensity due to a symmetry-allowed transition [$\lambda_{\text{max,calcd}} = 577$ nm, HOMO \rightarrow LUMO, $f = 0.1112$]. The above results suggest that the alternation of the orbital feature due to the ligand reorientation of the terminal CAASi ligands is reflected in the difference in intensities of the HOMO \rightarrow LUMO transitions.

Silylone **1** demonstrates the unprecedented molecular switch via electron redistribution between a low-valent silicon center and a redox noninnocent ligand which resembles that of transition metal complexes. From the structural point of view, the structural change between planar **1_p** and twisted **1_t** resembles that of the double-bond twisting of alkenes.²²

Steric and Electronic Effects on the Structure of Silylones. The reason for the presence of two stable isomers of **1** was investigated by theoretical calculations. This feature should be derived from the combination of steric and electronic effects, so various structurally related model silylones were calculated at the B3PW91-D3/B1 level of theory. Their relative Gibbs energies (298.15 K) were compared (Table 1: 6–9).²³ As discussed in the previous section, **1_t** and **1_p** were almost the same in relative Gibbs energies (**1_t** is slightly more stable by 0.2 kJ/mol than **1_p** in the gas phase, while **1_p** was slightly more stable by 4.3 kJ/mol than **1_t** in benzene). With this result as a reference, the steric effects were investigated. Hereafter, the suffix p for the compound number is referred to as a π -delocalized planar structure similar to **1_p** and the suffix t as a π -localized twisted structure similar to **1_t**. Although silylones **6_p** (N–Me) and **6_t** were both located as minima, the planar structure **6_p** was energetically favorable by 8.3 kJ/mol (gas phase), which implies that the twisted structure such as that seen for **1_t** might be a result of the bulky adamantyl substituents avoiding steric repulsion. This trend was more conspicuous for the bis(dialkylsilylene)-ligated silylones **A**, **7_p**, **7_t**, and **8_p**. While **A** only exhibits a twisted structure due to the severe steric demands of the two terminal five-membered rings, changing the two SiMe₃ moieties to sterically less demanding substituents resulted in the stabilization of the planar structure (**7_p** (SiH₃) and **8_p** (CH₃)).^{4e,g,6g} In fact, the π -localized twisted structure is not even located as a local minimum for **8**, which strongly suggests the importance of steric effects for the stabilization of the twisted structure.

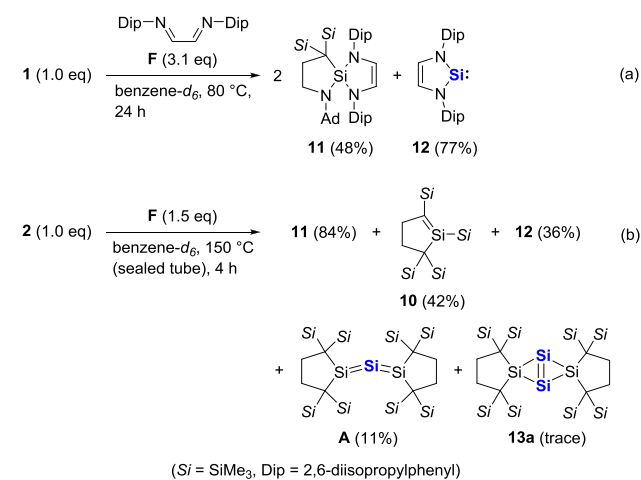
In contrast, heteroleptic silylones which are stabilized by CAASi **3** and CDASi **4** exhibit only π -localized twisted ylidene structures regardless of the substituents (**2_t** and **9_t**), and the corresponding planar structures could not be located as local

minima. Thus, the absence of a planar structure for **2** should be attributed to the energy difference between the vacant 3p orbitals of **3** and **4**: the lower-lying 3p orbital of **4** interacts more effectively with the LP(π) orbital to lower its energy level.^{4c} Consequently, **3** arranges perpendicular to **4** in order to stabilize the LP(σ) electrons to keep it lower in energy than the LP(π) orbital.

Thus, the switchable isomerization observed for **1** might be attributed to the stabilization of the π -localized ylidene structure by the balanced steric demand, crystal packing forces, as well as the electronic effects of the adjacent nitrogen atom of the azasilacyclopentane ring which results in the small energy gap between the π -localized and π -delocalized ylidene structures.

Monatomic Silicon Transfer Reactions. While silylone **1** was stable at room temperature in a benzene-*d*₆ solution, heating at 80 °C for 3 days yielded CAASi **3** (29%)²⁴ along with unidentified minor byproducts. Conversely, silylone **2** was stable even upon heating at 120 °C (sealed tube, benzene-*d*₆ solution). Eventually, heating at 150 °C for 3 days gave a complex mixture with signs of CAASi **3** (40%) and silene **10** (6%), a thermal isomerization product of CDASi **4**.¹⁰ These behaviors are different from that of **A** which does not decompose in the same conditions. This result prompted us to investigate the details of the formation of the silylone derivatives from **1** and **2**. Heating a benzene-*d*₆ solution of **1** in the presence of an alternative Lewis base, *N,N'*-bis(2,6-diisopropylphenyl)ethane-1,2-diimine (**F**, 3.1 equiv), at 80 °C afforded a mixture of triaminosilane **11** (48%)²⁴ and diaminosilylene **12**²⁵ (77%) (Scheme 5a). Triaminosilane **11** is

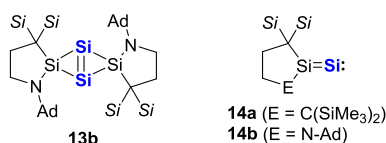
Scheme 5. Reactions of (a) 1 and (b) 2 with *N,N'*-Bis(2,6-diisopropylphenyl)ethane-1,2-diimine **F (Yields Determined by ¹H NMR Spectroscopy)²⁴**



a (1 + 4) cycloadduct of **3** and diimine **F**. Thus, the formation of diaminosilylene **12** implies that the two CAASi ligands have been eliminated from the central silicon atom of **1** and are likely to be exchanged by **F**, which could also be interpreted as a monatomic silicon transfer reaction. Insight into the mechanism of this reaction was obtained by the reaction of silylone **2** with **F**. Heating a benzene-*d*₆ solution of **2** in the presence of **F** (1.5 equiv)²⁶ at 150 °C afforded a mixture of triaminosilane **11** (84%),²⁴ silene **10** (42%), diaminosilylene **12** (36%), **A** (11%), and a trace amount of bicyclo[1.1.0]-tetrasil-1(3)-ene **13a**,²⁷ all of which were identified by

multinuclear NMR spectroscopy (Figures S36–S37) as well as HRMS (APCI) spectrometry (Figures S63–S72, Scheme 5b). A similar result was obtained for the reaction with *N,N'*-di(*t*-butyl)ethane-1,2-diimine (for details, see the Supporting Information). The formation of **10**, **11**, and **12** implies that silylenes **3** and **4** have both been eliminated from the central silicon atom of **2** and exchanged by **F**. Thus, it is reasonable to hypothesize that **A** should be obtained by the reaction of CDASi **4** with disilavinylidene intermediate **14a** (Chart 3)

Chart 3. Bicyclo[1.1.0]tetrasil-1(3)-ene 13b and Disilavinylidenes 14 (Si = SiMe₃)



which should generate after the elimination of **3**. Similarly, bicyclo[1.1.0]tetrasil-1(3)-ene **13a** should be obtained by dimerization of **14a**.²⁷ Notably, the thermolysis of **A** in the presence of **F** resulted in the full recovery of **A**. The aforementioned studies along with the absence of bicyclo[1.1.0]tetrasil-1(3)-ene **13b** and silylone **1** suggest that the ligand exchange reaction should proceed by a stepwise mechanism and likely via disilavinylidene intermediate **14a** rather than **14b**. The presence of the thermally stable CAASi **3** or the strong ylidene character of **1** and **2** should be the major driving force for the reaction to proceed.²⁸ Similar silicon transfer reactions were individually reported by Roesky^{29b} and Robinson's^{29a} group, but both involve the oxidation of the central silicon atom during the reactions. In contrast, oxidation is unnecessary for the reaction of **1** and **2**.³⁰

CONCLUSION

We have synthesized the first monatomic silicon complex (silylone) **1** that exhibits two stable isomers that could be reversibly switched by phase transfer. The structural, electronic, and physical properties were investigated by experimental and theoretical methods along with the heteroleptic silylone **2**. Silylone **1** in solution was suggested to be best described as the π -delocalized ylidene-type silylone in which the LP(π) electrons are delocalized across the Si–Si–Si skeleton, while **1** in the solid state and **2** should be best described as a π -localized ylidene-type silylone in which the LP(π) electrons are selectively delocalized to one of the terminal Si atoms. Delocalization of the LP(σ) of the central silicon atom to the Si atom of the silylene ligands results in weak but significant bent-allene character for **2** and **1** in the solid state. The drastic differences in the UV–vis absorption spectra observed between **1** in the solid state and in solution are attributed to the perpendicular and parallel orientation of the two terminal five-membered rings, respectively, which changes the relative intensity of the longest-wavelength absorption band (HOMO \rightarrow LUMO transition). Moreover, the ligand exchange and silicon atom transfer reactions of **1** and **2** were accomplished by thermal elimination of the terminal silylene ligands in the presence of ethane-1,2-diimines at high temperatures. The thermal stability of **3** and the ylidene character of the silylones should be the major driving forces for such reactions. The above studies should shed light on silylones or formally zerovalent group-14 element species as

fascinating research targets for molecular switches as well as monatomic group-14 element surrogates.

ASSOCIATED CONTENT

Supporting Information

The Supporting Information is available free of charge at <https://pubs.acs.org/doi/10.1021/jacs.1c06654>.

Experimental and theoretical details (PDF)

Atomic coordinates of optimized structures (XYZ)

NMR data (ZIP)

Accession Codes

CCDC 2091211–2091212 contain the supplementary crystallographic data for this paper. These data can be obtained free of charge via www.ccdc.cam.ac.uk/data_request/cif, or by emailing data_request@ccdc.cam.ac.uk, or by contacting The Cambridge Crystallographic Data Centre, 12 Union Road, Cambridge CB2 1EZ, UK; fax: +44 1223 336033.

AUTHOR INFORMATION

Corresponding Author

Takeaki Iwamoto – Department of Chemistry, Graduate School of Science, Tohoku University, Sendai 980-8578, Japan; orcid.org/0000-0002-8556-5785; Email: takeaki.iwamoto@tohoku.ac.jp

Authors

Taichi Koike – Department of Chemistry, Graduate School of Science, Tohoku University, Sendai 980-8578, Japan; orcid.org/0000-0002-6713-4375

Takumi Nukazawa – Department of Chemistry, Graduate School of Science, Tohoku University, Sendai 980-8578, Japan; orcid.org/0000-0001-6587-396X

Complete contact information is available at: <https://pubs.acs.org/10.1021/jacs.1c06654>

Notes

The authors declare no competing financial interest.

ACKNOWLEDGMENTS

This work was supported by the JSPS KAKENHI (grant JP20J21205 to T. K.; JP15K13634 to T. I.) and the Mitsubishi Foundation research grant in the natural sciences (201910006 to T.I.). The authors thank Prof. Shinya Takaishi and Mr. Shohei Koyama (Tohoku University) for helpful advice in the measurement of the solid-state UV–vis spectra.

REFERENCES

- (1) For some comprehensive reviews on silicon-based nanomaterials for biomedicine or nanodevices, see: (a) Zhang, D.-X.; Esser, L.; Vasani, R. B.; Thissen, H.; Voelcker, N. H. Porous Silicon Nanomaterials: Recent Advances in Surface Engineering for Controlled Drug-delivery Applications. *Nanomedicine* **2019**, *14*, 3213–3230. (b) Kafshgari, M. H.; Voelcker, N. H.; Harding, F. J. Applications of Zero-valent Silicon Nanostructures in Biomedicine. *Nanomedicine* **2015**, *10*, 2553–2571. (c) Peng, F.; Su, Y.; Zhong, Y.; Fan, C.; Lee, S.-T.; He, Y. Silicon Nanomaterials Platform for Bioimaging, Biosensing, and Cancer Therapy. *Acc. Chem. Res.* **2014**, *47*, 612–623. (d) Teo, B. K.; Sun, X. H. Silicon Based Low-Dimensional Nanomaterials and Nanodevices. *Chem. Rev.* **2007**, *107*, 1454–1532.
- (2) For reports on isolable diatomic and triatomic silicon species, see: (a) Mondal, K. C.; Roy, S.; Dittrich, B.; Andrada, D. M.; Frenking, G.; Roesky, H. W. A Triatomic Silicon(0) Cluster Stabilized

by a Cyclic Alkyl(amino) Carbene. *Angew. Chem., Int. Ed.* **2016**, *55*, 3158–3161. (b) Wang, Y.; Xie, Y.; Wei, P.; King, R. B.; Schaefer, H. F., III; Schleyer, P. v. R.; Robinson, G. H. A Stable Silicon(0) Compound with a Si = Si Double Bond. *Science* **2008**, *321*, 1069–1071.

(3) For some comprehensive reviews on divalent group-14 element species, see: (a) Shan, C.; Yao, S.; Driess, M. Where Silylene–silicon Centres Matter in the Activation of Small Molecules. *Chem. Soc. Rev.* **2020**, *49*, 6733–6754. (b) Zhou, Y.-P.; Driess, M. Isolable Silylene Ligands Can Boost Efficiencies and Selectivities in Metal-Mediated Catalysis. *Angew. Chem., Int. Ed.* **2019**, *58*, 3715–3728. (c) Nesterov, V.; Reiter, D.; Bag, P.; Frisch, P.; Holzner, R.; Porzelt, A.; Inoue, S. NHCs in Main Group Chemistry. *Chem. Rev.* **2018**, *118*, 9678–9842. (d) Hadlington, T. J.; Driess, M.; Jones, C. Low-valent Group 14 Element Hydride Chemistry: Towards Catalysis. *Chem. Soc. Rev.* **2018**, *47*, 4176–4197. (e) Weetman, C.; Inoue, S. The Road Travelled: After Main-Group Elements as Transition Metals. *ChemCatChem* **2018**, *10*, 4213–4228. (f) Raoufoghaddam, S.; Zhou, Y.-P.; Wang, Y.; Driess, M. N-heterocyclic Silylenes as Powerful Steering Ligands in Catalysis. *J. Organomet. Chem.* **2017**, *829*, 2–10. (g) Blom, B.; Gallego, D.; Driess, M. N-heterocyclic Silylene Complexes in Catalysis: New Frontiers in an Emerging Field. *Inorg. Chem. Front.* **2014**, *1*, 134–148. (h) Blom, B.; Stoelzel, M.; Driess, M. New Vistas in N-Heterocyclic Silylene (NHSi) Transition-Metal Coordination Chemistry: Syntheses, Structures and Reactivity towards Activation of Small Molecules. *Chem. - Eur. J.* **2013**, *19*, 40–62. (i) Yao, S.; Xiong, Y.; Driess, M. Zwitterionic and Donor-Stabilized N-Heterocyclic Silylenes (NHSis) for Metal-Free Activation of Small Molecules. *Organometallics* **2011**, *30*, 1748–1767. (k) Melaimi, M.; Soleilhavoup, M.; Bertrand, G. Stable Cyclic Carbenes and Related Species beyond Diaminocarbenes. *Angew. Chem., Int. Ed.* **2010**, *49*, 8810–8849. (l) Mizuhata, Y.; Sasamori, T.; Tokitoh, N. Stable Heavier Carbene Analogues. *Chem. Rev.* **2009**, *109*, 3479–3511. (m) Vignolle, J.; Cattoen, X.; Bourissou, D. Stable Noncyclic Singlet Carbenes. *Chem. Rev.* **2009**, *109*, 3333–3384.

(4) For important theoretical studies on silylones, see: (a) Turek, J.; Braidia, B.; De Proft, F. Bonding in Heavier Group 14 Zero-Valent Complexes—A Combined Maximum Probability Domain and Valence Bond Theory Approach. *Chem. - Eur. J.* **2017**, *23*, 14604–14613. (b) Niepötter, B.; Herbst-Irmer, R.; Kratzert, D.; Samuel, P. P.; Mondal, K. C.; Roesky, H. W.; Jerabek, P.; Frenking, G.; Stalke, D. Experimental Charge Density Study of a Silylone. *Angew. Chem., Int. Ed.* **2014**, *53*, 2766–2770. (c) Sarmah, S.; Guha, A. K.; Phukan, A. K.; Kumar, A.; Gadre, S. R. Stabilization of Si(0) and Ge(0) Compounds by Different Silylenes and Germynes: A Density Functional and Molecular Electrostatic Study. *Dalton Trans.* **2013**, *42*, 13200–13209. (d) Takagi, N.; Tonner, R.; Frenking, G. Carbodiphosphorane Analogues E(PPh₃)₂ with E = C–Pb: A Theoretical Study with Implications for Ligand Design. *Chem. - Eur. J.* **2012**, *18*, 1772–1780. (e) Kira, M.; Iwamoto, T.; Ishida, S.; Masuda, H.; Abe, T.; Kabuto, C. Unusual Bonding in Trisilaallene and Related Heavy Allenes. *J. Am. Chem. Soc.* **2009**, *131*, 17135–17144. (f) Takagi, N.; Shimizu, T.; Frenking, G. Divalent Silicon(0) Compounds. *Chem. - Eur. J.* **2009**, *15*, 3448–3456. (g) Kosa, M.; Karni, M.; Apeloig, Y. Trisilaallene and the Relative Stability of Si₃H₄ Isomers. *J. Chem. Theory Comput.* **2006**, *2*, 956–964.

(5) For definition of carbones, see: (a) Esterhuysen, C.; Frenking, G. Distinguishing Carbones from Allenes by Complexation to AuCl. *Chem. - Eur. J.* **2011**, *17*, 9944–9956. (b) Tonner, R.; Oxler, F.; Neumüller, B.; Petz, W.; Frenking, G. Carbodiphosphoranes: The Chemistry of Divalent Carbon(0). *Angew. Chem., Int. Ed.* **2006**, *45*, 8038–8042. For some reviews on carbones and their heavier-element analogues, see: (c) Majhi, P. K.; Sasamori, T. Tetrylones: An Intriguing Class of Monoatomic Zero-valent Group 14 Compounds. *Chem. - Eur. J.* **2018**, *24*, 9441–9455. (d) Zhao, L.; Hermann, M.; Holzmann, N.; Frenking, G. Dative Bonding in Main Group Compounds. *Coord. Chem. Rev.* **2017**, *344*, 163–204. (e) Yao, S.; Xiong, Y.; Driess, M. A New Area in Main-Group Chemistry: Zervalent Monoatomic Silicon Compounds and Their Analogues.

Acc. Chem. Res. **2017**, *50*, 2026–2037. (f) Petz, W. Addition Compounds between Carbones, CL₂, and Main Group Lewis Acids: A New Glance at Old and New Compounds. *Coord. Chem. Rev.* **2015**, *291*, 1–27.

(6) (a) Yao, S.; Kostenko, A.; Xiong, Y.; Ruzicka, A.; Driess, M. Redox Noninnocent Monoatomic Silicon(0) Complex (“Silylone”): Its One-Electron-Reduction Induces an Intramolecular One-Electron-Oxidation of Silicon(0) to Silicon(I). *J. Am. Chem. Soc.* **2020**, *142*, 12608–12612. (b) Wang, Y.; Karni, M.; Yao, S.; Kaushansky, A.; Apeloig, Y.; Driess, M. Synthesis of an Isolable Bis(silylene)-Stabilized Silylone and Its Reactivity Toward Small Gaseous Molecules. *J. Am. Chem. Soc.* **2019**, *141*, 12916–12927. (c) Sugahara, T.; Sasamori, T.; Tokitoh, N. Highly Bent 1,3-Digerma-2-silaallene. *Angew. Chem., Int. Ed.* **2017**, *56*, 9920–9923. (d) Xiong, Y.; Yao, S.; Inoue, S.; Epping, J. D.; Driess, M. A Cyclic Silylone (“Siladicarbene”) with an Electron-Rich Silicon(0) Atom. *Angew. Chem., Int. Ed.* **2013**, *52*, 7147–7150. (e) Mondal, K. C.; Roesky, H. W.; Schwarzer, M. C.; Frenking, G.; Niepötter, B.; Wolf, H.; Herbst-Irmer, R.; Stalke, D. A Stable Singlet Biradicaloid Siladicarbene: (L)₂Si. *Angew. Chem., Int. Ed.* **2013**, *52*, 2963–2967. (f) Iwamoto, T.; Masuda, H.; Kabuto, C.; Kira, M. Trigermaallene and 1,3-Digermasilaallene. *Organometallics* **2005**, *24*, 197–199. (g) Ishida, S.; Iwamoto, T.; Kabuto, C.; Kira, M. A Stable Silicon-based Allene Analogue with a Formally sp-Hybridized Silicon Atom. *Nature* **2003**, *421*, 725–727. For related species, see: (h) Keuter, J.; Hepp, A.; Mück-Lichtenfeld, C.; Lips, F. Facile Access to an NHC-Coordinated Silicon Ring Compound with a Si = N Group and a Two-Coordinate Silicon Atom. *Angew. Chem., Int. Ed.* **2019**, *58*, 4395–4399.

(7) For comprehensive reviews, see: (a) Tezgerevska, T.; Alley, K. G.; Boskovic, C. Valence Tautomerism in Metal Complexes: Stimulated and Reversible Intramolecular Electron Transfer between Metal Centers and Organic Ligands. *Coord. Chem. Rev.* **2014**, *268*, 23–40. (b) Sato, O.; Tao, J.; Zhang, Y.-Z. Control of Magnetic Properties through External Stimuli. *Angew. Chem., Int. Ed.* **2007**, *46*, 2152–2187. For some important studies, see: (c) Zaragoza, J. P. T.; Baglia, R. A.; Siegler, M. A.; Goldberg, D. P. Strong Inhibition of O-Atom Transfer Reactivity for Mn^V(O)(π -Radical-Cation)(Lewis Acid) versus Mn^V(O) Porphyrinoid Complexes. *J. Am. Chem. Soc.* **2015**, *137*, 6531–6540. (d) Buchanan, R. M.; Pierpont, C. G. Tautomeric Catecholate-Semiquinone Interconversion via Metal-Ligand Electron Transfer. Structural, Spectral, and Magnetic Properties of (3,5-Di-*tert*-butylcatecholato)-(3,5-di-*tert*-butylsemiquinone)-(bipyridyl)cobalt(III), a Complex Containing Mixed-Valence Organic Ligands. *J. Am. Chem. Soc.* **1980**, *102*, 4951–4957.

(8) For some reviews on molecular switches by electro-/pericyclic reactions, see: (a) Irie, M. Diarylethenes for Memories and Switches. *Chem. Rev.* **2000**, *100*, 1685–1716. (b) Berkovic, G.; Krongauz, V.; Weiss, V. Spiropyran and Spirooxazines for Memories and Switches. *Chem. Rev.* **2000**, *100*, 1741–1754. For some important studies, see: (c) Ravat, P.; Šolomek, T.; Häussinger, D.; Blacque, O.; Juríček, M. Dimethylcethrene: A Chiroptical Diradicaloid Photoswitch. *J. Am. Chem. Soc.* **2018**, *140*, 10839–10847. (d) Irie, M.; Kobatake, S.; Horichi, M. Reversible Surface Morphology Changes of a Photochromic Diarylethene Single Crystal by Photoirradiation. *Science* **2001**, *291*, 1769–1772. For some important studies on molecular switches by reversible dimerization, see: (e) Lekin, K.; Winter, S. M.; Downie, L. E.; Bao, X.; Tse, J. S.; Desgreniers, S.; Secco, R. A.; Dube, P. A.; Oakley, R. T. Hysteretic Spin Crossover between a Bisdithiazolyl Radical and Its Hypervalent σ -Dimer. *J. Am. Chem. Soc.* **2010**, *132*, 16212–16224. (f) Jutzi, P.; Mix, A.; Neumann, B.; Rummel, B.; Schoeller, W. W.; Stämmler, H.-G.; Rozhenko, A. B. Reversible Transformation of a Stable Monomeric Silicon(II) Compound into a Stable Disilene by Phase Transfer: Experimental and Theoretical Studies of the System {[(Me₃Si)₂N](Me₃C₃)Si]_n with n = 1, 2. *J. Am. Chem. Soc.* **2009**, *131*, 12137–12143. (g) Itkis, M. E.; Chi, X.; Cordes, A. W.; Haddon, R. C. Magneto-Opto-Electronic Bistability in a Phenalenyl Based Neutral Radical. *Science* **2002**, *296*, 1443–1445. (h) Hinchley, S. L.; Morrison, C. A.; Rankin, D. W. H.; Macdonald, C. L. B.; Wiacek, R. J.; Voigt, A.; Cowley, A. H.; Lappert,

M. F.; Gundersen, G.; Clyburne, J. A. C.; Power, P. P. Spontaneous Generation of Stable Pnictinyl Radicals from “Jack-in-the-Box” Dipnictines: A Solid-State, Gas-Phase, and Theoretical Investigation of the Origins of Steric Stabilization. *J. Am. Chem. Soc.* **2001**, *123*, 9045–9053. (i) Fujita, W.; Awaga, K. Room-Temperature Magnetic Bistability in Organic Radical Crystals. *Science* **1999**, *286*, 261–262.

(9) Kosai, T.; Ishida, S.; Iwamoto, T. A Two-Coordinate Cyclic (Alkyl)(amino)silylene: Balancing Thermal Stability and Reactivity. *Angew. Chem., Int. Ed.* **2016**, *55*, 15554–15558.

(10) Kira, M.; Ishida, S.; Iwamoto, T.; Kabuto, C. The First Isolable Dialkylsilylene. *J. Am. Chem. Soc.* **1999**, *121*, 9722–9723.

(11) Notably, the result of the reductive dehalogenation reaction of **5** was highly dependent on the concentration of the starting materials. Conducting the reaction in a lower concentration (a 50 mM THF solution of **5**) selectively afforded **A** along with free CAASi **3**, and **2** was not obtained. Although the precise cause of such selectivity is unclear at this point, the cleavage of the Si–Si bond of **5** might compete under low concentration.

(12) For some recent reviews on disilenes, see: (a) Präsang, C.; Scheschkewitz, D. Reactivity in the Periphery of Functionalised Multiple Bonds of Heavier Group 14 Elements. *Chem. Soc. Rev.* **2016**, *45*, 900–921. (b) Iwamoto, T.; Ishida, S. *In Functional Molecular Silicon Compounds II: Low Oxidation States*; Scheschkewitz, D., Ed.; Springer International Publishing: Cham, 2014; pp 125–202. (c) Kira, M. Bonding and Structure of Disilenes and Related Unsaturated Group-14 Element Compounds. *Proc. Jpn. Acad., Ser. B* **2012**, *88*, 167–191. (d) Fischer, R. C.; Power, P. P. π -Bonding and the Lone Pair Effect in Multiple Bonds Involving Heavier Main Group Elements: Developments in the New Millennium. *Chem. Rev.* **2010**, *110*, 3877–3923. (e) Kira, M.; Iwamoto, T. Progress in the Chemistry of Stable Disilenes. *Adv. Organomet. Chem.* **2006**, *54*, 73–148.

(13) Kosai, T.; Iwamoto, T. Stable Push–Pull Disilene: Substantial Donor–Acceptor Interactions through the Si=Si Double Bond. *J. Am. Chem. Soc.* **2017**, *139*, 18146–18149.

(14) (a) Ghana, P.; Arz, M. I.; Das, U.; Schnakenburg, G.; Filippou, A. C. Si = Si Double Bonds: Synthesis of an NHC-Stabilized Disilavinylidene. *Angew. Chem., Int. Ed.* **2015**, *54*, 9980–9985. For other related species, see: (b) Li, Y.; Chan, Y.-C.; Li, Y.; Purushothaman, I.; De, S.; Parameswaran, P.; So, C.-W. Synthesis of a Bent 2-Silaallene with a Perturbed Electronic Structure from a Cyclic Alkyl(amino) Carbene-Diiodosilylene. *Inorg. Chem.* **2016**, *55*, 9091–9098. (c) Kobayashi, R.; Ishida, S.; Iwamoto, T. Synthesis of an NHC-Coordinated Dialkyldisilavinylidene and Its Oxidation Providing a Silicon Analog of an Acetolactone. *Organometallics* **2021**, *40*, 843–847.

(15) Koyama, S.; Tanabe, T.; Takashi, S.; Yamashita, M.; Iguchi, H. Preliminary Chemical Reduction for Synthesizing a Stable Porous Molecular Conductor with Neutral Metal Nodes. *Chem. Commun.* **2020**, *56*, 13109–13112.

(16) For the details of the TD-DFT calculations conducted for silylones **1**, **2**, and **A**, see the [Supporting Information](#).

(17) The difference in electronic energy between I_p and I_t was small regardless of the calculation level ($\Delta E (= E(I_t) - E(I_p)) = 3.8$ kJ/mol at the DLPNO-CCSD(T)/def2-TZVP level of theory; $\Delta E = 2.0$ kJ/mol at the B3PW91-D3/B1 level of theory). The B3PW91-D3/B1 level was used considering the calculation costs.

(18) For the details of the GIAO calculations conducted for silylones **1**, **2**, and **A**, see the [Supporting Information](#).

(19) In the case of I_t and I_p , resonance structures representing negative hyperconjugation in ylidene structures ($LP(\sigma, Si_2) \rightarrow \sigma^*(Si-N)$) were found as major contributors (I_t : 15.2%, I_p : 2 \times 24.8%). For details, see Figure S100 in the [SI](#).

(20) NLMO and NBO analyses are used to finely explain the electronic properties of bis(silylene)-stabilized silylones and germylones previously reported by Driess, Apeloig, and co-workers. For reference, see: Wang, Y.; Karni, M.; Yao, S.; Apeloig, Y.; Driess, M. An Isolable Bis(silylene)-Stabilized Germylone and Its Reactivity. *J. Am. Chem. Soc.* **2019**, *141*, 1655–1664. See also, ref [6b](#).

(21) The band positions and intensities of **2_t** were qualitatively in good agreement with those obtained from the experimental spectrum, but the longest absorption wavelength was overestimated which is an intramolecular charge-transfer-type transition. Calculated absorption wavelengths for intramolecular charge transfer transition of disilenes are reported to largely differ from the observed wavelengths. For studies, see: Kosai, T.; Ishida, S.; Iwamoto, T. Heteroaryl disilenes: Heteroaryl Groups Serve as Electron Acceptors for Si = Si Double Bonds in Intramolecular Charge Transfer Transitions. *Dalton Trans.* **2017**, *46*, 11271–11281.

(22) For some important studies on reversible twisting of double bonds of alkenes, see: (a) Kostenko, A.; Tumanskii, B.; Karni, M.; Inoue, S.; Ichinohe, M.; Sekiguchi, A.; Apeloig, Y. Observation of a Thermally Accessible Triplet State Resulting from Rotation around a Main-Group π Bond. *Angew. Chem., Int. Ed.* **2015**, *54*, 12144–12148. (b) Takezawa, H.; Murase, T.; Fujita, M. Temporary and Permanent Trapping of the Metastable Twisted Conformer of an Overcrowded Chromic Alkene via Encapsulation. *J. Am. Chem. Soc.* **2012**, *134*, 17420–17423. (c) Browne, W. R.; Pollard, M. M.; de Lange, B.; Meetsma, A.; Feringa, B. L. Reversible Three-State Switching of Luminescence: A New Twist to Electro- and Photochromic Behavior. *J. Am. Chem. Soc.* **2006**, *128*, 12412–12413. (d) Koumura, N.; Zijlstra, R. W. J.; van Delden, R. A.; Harada, N.; Feringa, B. L. Light-driven Monodirectional Molecular Rotor. *Nature* **1999**, *401*, 152–155.

(23) The selected Kohn–Sham orbitals of silylones **6–9** are shown in [Figures S90–S95](#).

(24) The yields for the thermal reaction of **1** were calculated assuming that 2 equiv of products arising from **3** such as **11** as well as 1 equiv of a product arising from the central silicon atom such as **12** theoretically form. Similarly, the yields for the thermal reaction of **2** were calculated assuming that 1 equiv of products arising from **3**, **4**, and the central silicon atom such as **12** theoretically forms, respectively.

(25) Zark, P.; Schafer, A.; Mitra, A.; Haase, D.; Saak, W.; West, R.; Muller, T. Synthesis and Reactivity of N-Aryl Substituted N-Heterocyclic Silylenes. *J. Organomet. Chem.* **2010**, *695*, 398–408.

(26) Diaminosilylene **12** was obtained in the highest yield when 1.5 equiv of **F** was used. The reaction of **2** with an excess amount of diimine **F** (5.0 equiv) provided a complex mixture.

(27) (a) Nukazawa, T.; Kosai, T.; Honda, S.; Ishida, S.; Iwamoto, T. Reactions of a Tetrasilabicyclo[1.1.0]but-1(3)-ene with Carbon Tetrachloride and Methanol. *Dalton Trans.* **2019**, *48*, 10874–10880. (b) Iwamoto, T.; Abe, T.; Sugimoto, K.; Hashizume, D.; Matsui, H.; Kishi, R.; Nakano, M.; Ishida, S. A Tetrasilicon Analogue of Bicyclo[1.1.0]but-1(3)-ene Containing a Si = Si Double Bond with an Inverted Geometry. *Angew. Chem., Int. Ed.* **2019**, *58*, 4371–4375.

(28) We previously reported that **3** could be eliminated from a cyclotrisilene likely due to the high thermal stability of **3**: Koike, T.; Honda, S.; Ishida, S.; Iwamoto, T. [1 + 2] Cycloaddition of a Cyclic (Alkyl)(amino)silylene and a Disilyne Providing a 3-Aminocyclotrisilene. *Organometallics* **2020**, *39*, 4149–4152.

(29) (a) Wang, Y.; Tope, C. A.; Xie, Y.; Wei, P.; Urbauer, J. L.; Schaefer, H. F., III; Robinson, G. H. Carbene-Stabilized Disilicon as a Silicon-Transfer Agent: Synthesis of a Dianionic Silicon Tris(dithiolene) Complex. *Angew. Chem., Int. Ed.* **2020**, *59*, 8864–8867. (b) Mondal, K. C.; Samuel, P. P.; Tretiakov, M.; Singh, A. P.; Roesky, H. W.; Stückl, A. C.; Niepötter, B.; Carl, E.; Wolf, H.; Herbst-Irmer, R.; Stalke, D. Easy Access to Silicon(0) and Silicon(II) Compounds. *Inorg. Chem.* **2013**, *52*, 4736–4743. For related studies, see: (c) Blom, B.; Said, A.; Szilvasi, T.; Menezes, P. W.; Tan, G.; Baumgartner, J.; Driess, M. Alkaline-Earth-Metal-Induced Liberation of Rare Allotropes of Elemental Silicon and Germanium from N-Heterocyclic Metallylenes. *Inorg. Chem.* **2015**, *54*, 8840–8848.

(30) The reaction of **2** with N-heterocyclic carbenes (NHCs) was examined, but no sign of NHC-ligated products was observed. For example, the reaction of **2** with 1,3-bis(2,6-diisopropylphenyl)imidazol-2-ylidene (1.5 equiv) afforded a mixture of silylene **3** (43%), **13a** (19%), and **A** (<8% due to signal overlap).